ChemComm

CrossMark
← click for updates

Structural transition and superconductivity in hydrothermally synthesized FeX (X = S, Se)†

U. Pachmayr, N. Fehn and D. Johrendt*

Iron selenide obtained by mild hydrothermal reaction is not superconducting and exhibits a triclinic crystal structure below 60 K unlike superconducting FeSe from conventional solid state synthesis which is orthorhombic. In contrast, tetragonal iron sulphide FeS from hydrothermal synthesis is superconducting but undergoes no structural change on cooling.

Unconventional superconductivity in iron arsenides and selenides with layered crystal structures and transition temperatures (T_c) up to 56 K in bulk phases[1–3] or even more exciting 100 K in thin FeSe films[4] triggers enormous interest in the scientific community.[5–9] One of the most intriguing traits of these materials is that superconductivity coexists or competes with other types of electronic, magnetic, or structural orders that may or may not directly couple to superconductivity.[10,11] Most of the iron arsenides, among them LaOFeAs and $BaFe_2As_2$ traverse tetragonal-to-orthorhombic phase transitions accompanied by antiferromagnetic order.[12,13] Superconductivity emerges during suppression of the magnetic order by doping or pressure, and the highest critical temperatures occur in the undistorted tetragonal phases. Such a structural transition also occurs in the iron chalcogenide FeSe with tetragonal *anti*-PbO type structure,[14] but no magnetic order follows. This was quite surprising since magnetism was believed to be the driving force for the lattice distortion in iron arsenides (spin-nematic),[15,16] and moreover, magnetic fluctuations were considered as important for the formation of the Cooper pairs. Recent studies conclude that the structural transition in FeSe has no magnetic origin but is a consequence of orbital ordering (orbital-nematic)[16] with an unequal occupation of the iron $3d_{xz}/3d_{yz}$ orbitals.[17,18] The latest results suggest that orbital ordering and superconductivity compete in FeSe at low temperatures.[18] Thus superconducting, orbital and structural order parameters are uniquely intertwined and

display the signature of unconventional superconductivity in FeSe. This is in line with the fact that the relatively low T_c of 8 K in pure FeSe strongly increases under pressure to 36 K and by intercalation with molecular[19] or other species to 43 K.[20,21]

Recently Lai *et al.* reported that also the iron sulphide FeS with *anti*-PbO structure (mackinawite) is superconducting at 5 K if synthesized by a hydrothermal process.[22] So far all efforts made to pursue superconductivity in FeS from conventional synthesis failed. However, the complexity of the Fe–S phase diagram makes the synthesis of stoichiometric FeS difficult. Contrary to FeSe, several polymorphs of FeS are known,[23,24] where mackinawite has nearly FeS composition ($Fe_{1+x}S$, $0 < x < 0.07$).[25,26] Thus, one might assume that only the low-temperature hydrothermal process as used by Lai *et al.* produces stoichiometric FeS which is not accessible by conventional high-temperature routes.

Given the above scenario of FeSe the question arises, whether superconductivity in FeS also occurs in an orthorhombic phase as in the selenide. This would be a strong hint to unconventional pairing, and thus to the potential of FeS to exhibit much higher critical temperatures upon intercalation or other chemical modification. The unexpected observation of superconductivity in iron sulphide motivated us to study the low temperature crystal structures of both FeSe and FeS synthesized under mild hydrothermal conditions.

Fig. 1 shows the X-ray powder pattern of FeSe obtained by the hydrothermal reaction method,‡ referred to as $FeSe_{hydro}$ in the following. The Rietveld-analysis was carried out using the structural model of *anti*-PbO type FeSe. No impurity phases occur within the experimental limits ($\sim 1\%$ of a crystalline phase). Chemical analysis by ICP-AAS confirmed the stoichiometry $Fe_{1.02(1)}Se$ and $Fe_{1.01(1)}Se$ for $FeSe_{hydro}$ and conventionally synthesized FeSe ($FeSe_{conv}$), respectively. Crystallographic parameters are listed in Table 1 together with data for $FeSe_{conv}$. The lattice parameters and the selenium z positions are mutually the same, thus both crystal structures are identical from the view of X-ray powder diffraction. Neither chemical nor structural analysis revealed any evidence for iron vacancies in our $FeSe_{hydro}$ samples. It is known that deviations from the ideal composition interfere

Department Chemie, Ludwig-Maximilians-Universität München, Butenandtstr. 5-13 (D), 81377 München, Germany. E-mail: johrendt@lmu.de

† Electronic supplementary information (ESI) available: Crystallographic data of FeS, Rietveld-fits and structural data for $FeSe_{hydro}$ at 10 K, SEM images. See DOI: 10.1039/c5cc07739g
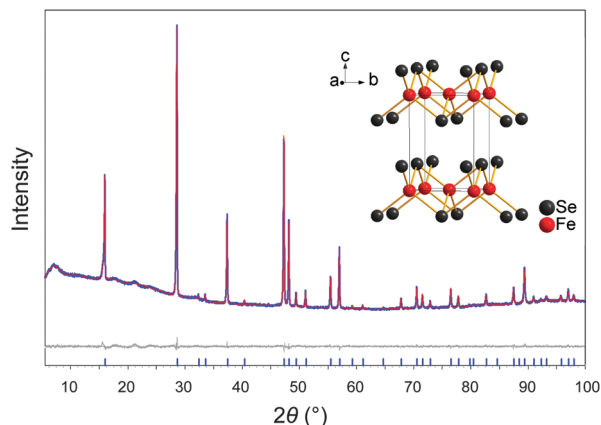
Fig. 1 X-ray powder pattern of FeSe synthesized *via* hydrothermal reaction method (blue) with Rietveld-fit (red) and difference plot (grey). Inset: Crystal structure of *anti*-PbO type FeSe. Broad features near 20° and below 10° are artefacts of the sample holder.

Fig. 2 Low-temperature *ac*-susceptibility of FeSe samples obtained by conventional (blue) and by hydrothermal synthesis (black).

Table 1 Crystallographic data of FeX (X = S, Se)

	FeSe$_{hydro}$	FeSe$_{conv}$	FeS$_{hydro}$
Space group	$P4/nmm$ (No. 129, O2)		
a (pm)	377.11(1)	377.09(1)	368.18(1)
c (pm)	552.14(1)	552.16(1)	502.97(2)
Volume (nm^3)	0.07852(1)	0.07852(1)	0.06818(1)
Positions	2 Fe at 2a ($\frac{3}{4}$, $\frac{1}{4}$, 0)		
	2 Se(S) at 2c ($\frac{1}{4}$, $\frac{1}{4}$, z)		
	z = 0.2672(2)	z = 0.2669(2)	z = 0.262(1)
Phase fractions (wt%) and R-values			
Fe$X_{(PbO-type)}$	100	93.6	100
Fe$X_{(NiAs-type)}$	0	6.4	0
R_{wp}	1.21	1.01	1.81
R_{exp}	1.09	0.85	1.22
χ^2	1.11	1.19	1.49
Atomic distances (pm) and angles (°)			
Fe–Fe	266.66(1) × 4	266.64(1) × 4	260.3(1) × 4
Fe–X	239.31(3) × 4	239.40(3) × 4	226.5(3) × 4
X–Fe–X	103.93(1) × 2	103.97(1) × 2	108.8(1) × 2
	112.31(1) × 4	112.29(1) × 4	109.8(1) × 4

with superconductivity in Fe$_{1+\delta}$Se (δ = 0.03) from solid state synthesis[27] as well as in Fe$_{1-\delta}$Se (δ = 0.1) from solvothermal reactions.[28] Our data reveals ideal stoichiometric FeSe$_{hydro}$ and gives no reason against superconductivity.

The *ac*-susceptibilities of the FeSe samples are surprisingly different (Fig. 2). While the expected bulk superconductivity occurs near 8 K in the conventionally synthesized sample, only traces of superconductivity are visible in the sample from hydrothermal synthesis. Since no differences in composition or structure were detected at room temperature, next we have determined the low-temperature crystal structures.

Fig. 3 shows the temperature dependency of the lattice parameters. The structural transition from tetragonal ($P4/nmm$) to orthorhombic ($Cmme$) symmetry occurs near 90 K in FeSe$_{conv}$ in good agreement with published data.[14,29] The transition temperature is significantly lower in the hydrothermally synthesized sample, where the lattice parameters split near 60 K.
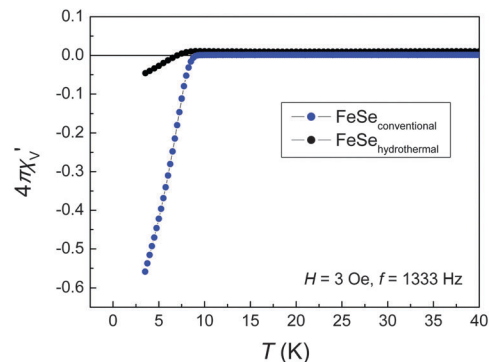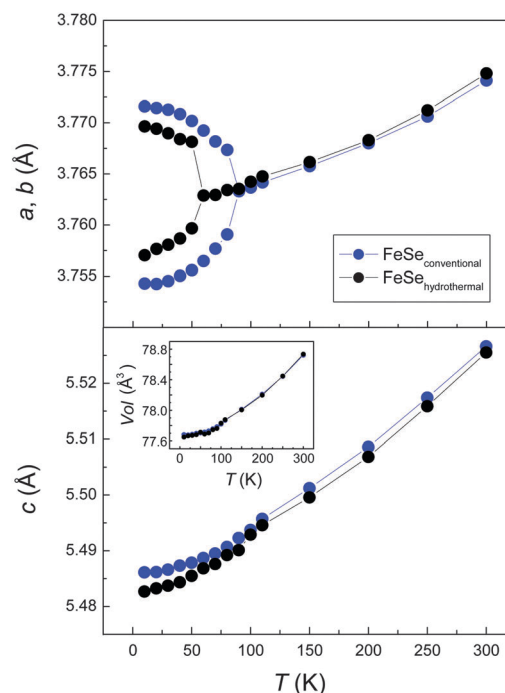

Fig. 3 Temperature dependency of the lattice constants in FeSe synthesized *via* hydrothermal (black) and conventional (blue) reaction method, respectively. The *a* and *b* lattice constants are divided by $\sqrt{2}$ at temperatures below the tetragonal-to-orthorhombic phase transition for the *Cmme* structure of FeSe$_{conv}$.

A detailed inspection of the diffraction pattern reveals an asymmetric splitting of some reflections in FeSe$_{hydro}$. Fig. 4 shows profiles of the $(220)_{tetra}$ Bragg reflection of the tetragonal phase that splits into a doublet during the phase transition. Their intensities have to be equal by symmetry if the structure is orthorhombic, which is true for FeSe$_{conv}$ but not for FeSe$_{hydro}$. The asymmetric profile cannot be fitted with a mixture of tetragonal ($P4/nmm$) and orthorhombic ($Cmme$) FeSe (Fig. S2, ESI†). Such a mixture is moreover unlikely because the transition to the *Cmme* structure should be at 90 K instead of 60 K as observed here. Thus there is strong evidence that the low-temperature structure of hydrothermally synthesized FeSe is different from the *Cmme* structure and has lower lattice symmetry.
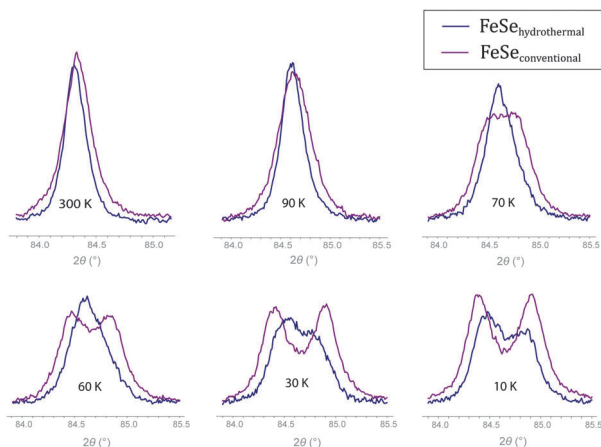
Fig. 4 Temperature evolution of the $(220)_{tetra}$ Bragg reflection splitting into doublets for FeSe synthesized *via* hydrothermal (blue) and conventional (magenta) reaction methods, respectively.

Subsequent Rietveld refinements yielded a triclinic structure ($P\bar{1}$) at 10 K with lattice parameters a = 376.59(2) pm, b = 376.66(2) pm and c = 547.93(1) pm. The α angle remains close to 90° (90.024(4)°), β and γ alter into 89.943(4)° and 90.168(2)°, respectively. The complete Rietveld fit and crystallographic data are given in the ESI† (Fig. S1 and Table S1). The resulting crystal structure differs significantly from superconducting FeSe$_{conv}$ and exhibits another distortion motif of the iron atoms, as depicted in Fig. 5. In the known orthorhombic low-temperature structure, iron atoms form stripes running along the shorter axis. The four identical Fe–Fe bonds in the tetragonal phase split into two slightly shorter (265.9 pm) and two longer ones (267.2 pm),[30] however, this difference is rather small. In the new structure of hydrothermally synthesized non superconducting FeSe$_{hydro}$ we observe iron atoms in zigzag-chains with short Fe–Fe bonds (256.9(2), 257.7(2) pm), while the distances between neighbouring chains become long (275.2(2) pm, 276.0(2) pm). Thus the structural transition in FeSe$_{hydro}$ leads to significantly enhanced Fe–Fe bonds in the zigzag chains, while the distortion in FeSe$_{conv}$ is much weaker and the Fe–Fe bonds remain longer.

These intriguing different crystal structures may be the reason for the absence of superconductivity in hydrothermally
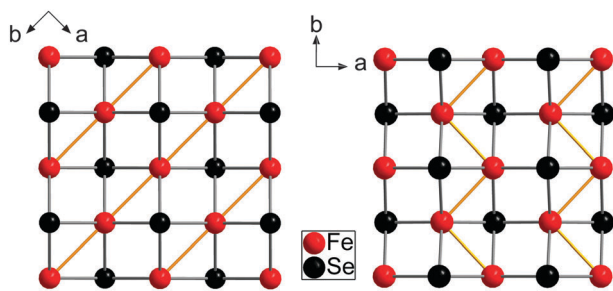
prepared FeSe. Currently it is accepted that the tiny distortion of FeSe$_{conv}$ is a result of orbital ordering, which is believed to be related to superconductivity.[18] From our results we suggest that the stronger distortion in FeSe$_{hydro}$ is rather driven by Fe–Fe bond formation, which may suppresses superconductivity. This is in line with the absence of magnetic ordering in FeSe$_{hydro}$ in contrast to antiferromagnetism present in non superconducting Fe$_{1-\delta}$Se[28] and Fe$_{1+\delta}$Te.[31] However, even if the absence of superconductivity in FeSe$_{hydro}$ may finally be traced back to the different crystal structure, it remains unclear why the obviously identical room temperature FeSe phases transform to different low-temperature structures.

If superconductivity in FeSe only occurs in the orthorhombic phase, the question arises if this is also the case in the newly discovered superconducting FeS. We have synthesized the iron sulphide using a similar hydrothermal procedure recently described by Lai *et al.*[22] X-ray powder diffraction revealed single-phase samples of FeS with *anti*-PbO type structure. The lattice parameters a = 368.18(1) pm and c = 502.97(2) pm are in good agreement with those reported in the literature.[32–35] Additional X-ray single-crystal analysis confirms the tetragonal structure (Table S2, ESI†). Our samples show superconductivity at 4.5–5 K (Fig. 6). Hydrothermal conditions turned out to be perfectly convenient to realize high quality FeS in a simple synthesis.

Fig. 7 shows the temperature dependencies of the lattice parameters. The unit cell shrinks on cooling without any appreciable anomalies. No broadening or splitting of the reflections is
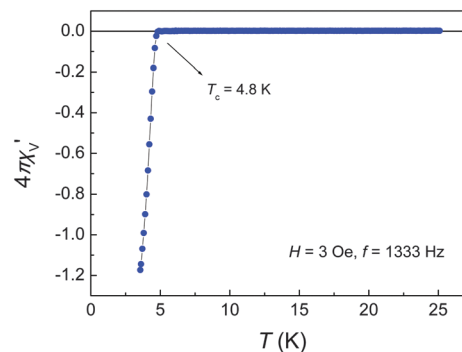

Fig. 6 Low-temperature *ac*-susceptibility of FeS.

Fig. 5 Low-temperature phase of FeSe synthesized *via* conventional (left) and hydrothermal (right) method. Iron stripes respectively iron zigzag chains are formed by short and large Fe–Fe distances.
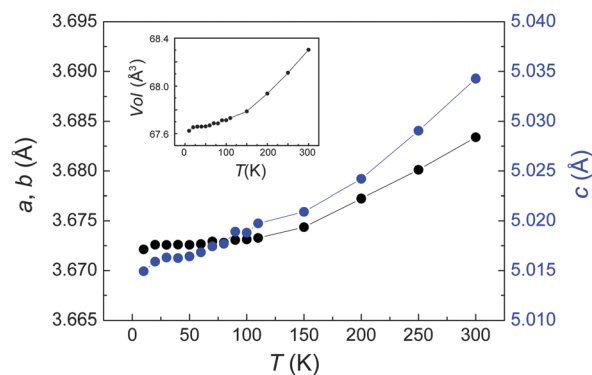

Fig. 7 Lattice parameters and unit cell volume (inset) of tetragonal FeS.

observed down to 10 K. Thus, contrary to FeSe, superconductivity in FeS emerges in the tetragonal phase. This is reminiscent of LaOFeP and LaOFeAs. While the phosphide is a conventional superconductor with T_c near 4 K, the arsenide is a parent compound of the high-T_c materials and exhibits magnetic fluctuations as well as a structural distortion. The absence of a transition in FeS suggests that no electronic spin or orbital ordering is present, which is according to recent findings related to unconventional superconductivity. This indicates that FeS may be a conventional superconductor in contrast to FeSe.

Finally it remains intriguing that hydrothermal synthesis under mild conditions yields superconducting FeS but non superconducting FeSe, while the opposite is true for high-temperature solid state methods. While stoichiometric FeS is probably only accessible by the hydrothermal method due to the complex phase diagram, we currently have no explanation for the surprising differences of the structures and properties between the FeSe samples at low temperatures.

Notes and references

1 D. C. Johnston, *Adv. Phys.*, 2010, **59**, 803–1061.
2 G. R. Stewart, *Rev. Mod. Phys.*, 2011, **83**, 1589–1652.
3 D. Johrendt, *J. Mater. Chem.*, 2011, **21**, 13726–13736.
4 J.-F. Ge, Z.-L. Liu, C. Liu, C.-L. Gao, D. Qian, Q.-K. Xue, Y. Liu and J.-F. Jia, *Nat. Mater.*, 2015, **14**, 285–289.
5 X. H. Chen, T. Wu, G. Wu, R. H. Liu, H. Chen and D. F. Fang, *Nature*, 2008, **453**, 761–762.
6 P. Cheng, B. Shen, G. Mu, X. Zhu, F. Han, B. Zeng and H.-H. Wen, *EPL (Europhysics Letters)*, 2009, **85**, 67003.
7 Y. Kamihara, T. Watanabe, M. Hirano and H. Hosono, *J. Am. Chem. Soc.*, 2008, **130**, 3296–3297.
8 R. H. Liu, G. Wu, T. Wu, D. F. Fang, H. Chen, S. Y. Li, K. Liu, Y. L. Xie, X. F. Wang, R. L. Yang, L. Ding, C. He, D. L. Feng and X. H. Chen, *Phys. Rev. Lett.*, 2008, **101**, 087001.
9 M. Rotter, M. Tegel and D. Johrendt, *Phys. Rev. Lett.*, 2008, **101**, 107006.
10 R. M. Fernandes and J. Schmalian, *Phys. Rev. B*, 2010, **82**, 014521.
11 R. M. Fernandes, A. V. Chubukov and J. Schmalian, *Nat. Physics*, 2014, **10**, 97–104.
12 C. de la Cruz, Q. Huang, J. W. Lynn, J. Y. Li, W. Ratcliff, J. L. Zarestky, H. A. Mook, G. F. Chen, J. L. Luo, N. L. Wang and P. C. Dai, *Nature*, 2008, **453**, 899–902.
13 M. Rotter, M. Tegel, I. Schellenberg, W. Hermes, R. Pöttgen and D. Johrendt, *Phys. Rev. B*, 2008, **78**, 020503(R).
14 T. M. McQueen, A. J. Williams, P. W. Stephens, J. Tao, Y. Zhu, V. Ksenofontov, F. Casper, C. Felser and R. J. Cava, *Phys. Rev. Lett.*, 2009, **103**, 057002–057004.
15 A. E. Böhmer and C. Meingast, *C. R. Phys.*, 2015, DOI: 10.1016/j.crhy.2015.07.001.
16 W. Zhentao and H. N. Andriy, *J. Phys.: Condens. Matter*, 2015, **27**, 225602.
17 T. Shimojima, Y. Suzuki, T. Sonobe, A. Nakamura, M. Sakano, J. Omachi, K. Yoshioka, M. Kuwata-Gonokami, K. Ono, H. Kumigashira, A. E. Boehmer, F. Hardy, T. Wolf, C. Meingast, H. V. Loehneysen, H. Ikeda and K. Ishizaka, *Phys. Rev. B*, 2014, **90**, 121111.
18 S. H. Baek, D. V. Efremov, J. M. Ok, J. S. Kim, J. van den Brink and B. Büchner, *Nat. Mater.*, 2015, **14**, 210–214.
19 M. Burrard-Lucas, D. G. Free, S. J. Sedlmaier, J. D. Wright, S. J. Cassidy, Y. Hara, A. J. Corkett, T. Lancaster, P. J. Baker, S. J. Blundell and S. J. Clarke, *Nat. Mater.*, 2013, **12**, 15–19.
20 U. Pachmayr, F. Nitsche, H. Luetkens, S. Kamusella, F. Brückner, R. Sarkar, H.-H. Klauss and D. Johrendt, *Angew. Chem., Int. Ed.*, 2015, **54**, 293–297.
21 U. Pachmayr and D. Johrendt, *Chem. Commun.*, 2015, **51**, 4689–4692.
22 X. Lai, H. Zhang, Y. Wang, X. Wang, X. Zhang, J. Lin and F. Huang, *J. Am. Chem. Soc.*, 2015, **137**, 10148–10151.
23 A. R. Lennie, S. A. T. Redfern, P. F. Schofield and D. J. Vaughan, *Mineral. Mag.*, 1995, **59**, 677–683.
24 S. D. Scott, *Rev. Mineral.*, 1974, **1**, S1–S38.
25 A. R. Lennie, S. A. T. Redfern, P. E. Champness, C. P. Stoddart, P. F. Schofield and D. J. Vaughan, *Am. Mineral.*, 1997, **82**, 302–309.
26 D. J. Vaughan and J. R. Craig, *Mineral chemistry of metal sulfides*, Cambridge University Press, 1978.
27 T. M. McQueen, Q. Huang, V. Ksenofontov, C. Felser, Q. Xu, H. Zandbergen, Y. S. Hor, J. Allred, A. J. Williams, D. Qu, J. Checkelsky, N. P. Ong and R. J. Cava, *Phys. Rev. B*, 2009, **79**, 014522–014527.
28 J. T. Greenfield, S. Kamali, K. Lee and K. Kovnir, *Chem. Mater.*, 2015, **27**, 588–596.
29 S. Margadonna, Y. Takabayashi, M. T. McDonald, K. Kasperkiewicz, Y. Mizuguchi, Y. Takano, A. N. Fitch, E. Suard and K. Prassides, *Chem. Commun.*, 2008, 5607–5609.
30 K. Horigane, H. Hiraka and K. Ohoyama, *J. Phys. Soc. Jpn.*, 2009, **78**, 074718.
31 Y. Mizuguchi and Y. Takano, *Z. Kristallogr.*, 2011, **226**, 417–434.
32 S. J. Denholme, S. Demura, H. Okazaki, H. Hara, K. Deguchi, M. Fujioka, T. Ozaki, T. Yamaguchi, H. Takeya and Y. Takano, *Mat. Chem. Phys.*, 2014, **147**, 50–56.
33 S. J. Denholme, H. Okazaki, S. Demura, K. Deguchi, M. Fujioka, T. Yamaguchi, H. Takeya, M. ElMassalami, H. Fujiwara, T. Wakita, T. Yokoya and Y. Takano, *Sci. Technol. Adv. Mater.*, 2014, **15**, 055007.
34 Z. Shu-Lin, W. Hui-Xian and D. Cheng, *Chin. Phys. B*, 2014, **23**, 087203.
35 I. T. Sines, D. D. Vaughn Ii, R. Misra, E. J. Popczun and R. E. Schaak, *J. Solid State Chem.*, 2012, **196**, 17–20.
36 A. Coelho, *TOPAS-Academic, V 4.1, Coelho Software*, Brisbane, 2007.
37 V. Petricek, M. Dusek and L. Palatinus, *Z. Kristallogr.*, 2014, **229**, 345–352.